Monte Carlo simulation of the Heisenberg antiferromagnet on a triangular lattice: Topological excitations

M. Wintel and H. U. Everts

Institut für Theoretische Physik, Universität Hannover, Appelstrasse 2, D-30167 Hannover, Germany

W. Apel

Physikalisch-Technische Bundesanstalt, Bundesallee 100, D-38116 Braunschweig, Germany

We have simulated the classical Heisenberg antiferromagnet on a triangular lattice using a local Monte Carlo algorithm. The behavior of the correlation length ξ, the susceptibility at the ordering wave vector $\chi(\mathbf{Q})$, and the spin stiffness ρ clearly reflects the existence of two temperature regimes—a high-temperature regime $T > T_{\rm th}$, in which the disordering effect of vortices is dominant, and a low-temperature regime $T < T_{\rm th}$, where correlations are controlled by small amplitude spin fluctuations. As has previously been shown, in the last regime, the behavior of the above quantities agrees well with the predictions of a renormalization-group treatment of the appropriate nonlinear σ model. For $T > T_{\rm th}$, a satisfactory fit of the data is achieved, if the temperature dependence of ξ and $\chi(\mathbf{Q})$ is assumed to be of the form predicted by the Kosterlitz-Thouless theory. Surprisingly, the crossover between the two regimes appears to happen in a very narrow temperature interval around $T_{\rm th} \simeq 0.28$.

I. INTRODUCTION

Magnetic ordering phenomena of both classical and quantum antiferromagnets on non-bipartite lattices are a fascinating subject. The simplest and most frequently studied model of this type is the Heisenberg antiferromagnet on a triangular lattice (HAFT). While the question of whether or not the typical features of this model have been observed in experiments is still a controversial issue,[1] the theoretical understanding of these features has advanced rapidly during recent years.[2-6] In contrast to antiferromagnets on bipartite lattices, the HAFT exhibits noncollinear magnetic order in its classical and most likely also in its quantum ground state. As a consequence, the order parameter of the HAFT is represented locally by a set of three mutually orthogonal unit vectors or, alternatively, by a rotation matrix which defines the local orientation of this set relative to some fixed frame of reference. Renormalization-group (RG) studies of appropriate nonlinear sigma (NLσ) models[3,4] have revealed a number of interesting properties of the HAFT. The symmetry of the model was found to be dynamically enhanced from $O(3) \otimes O(2)$ to $O(4)$, and in a two-loop RG calculation for the classical HAFT,[3] the temperature dependence of the correlation length ξ was obtained as

$$\xi = \Delta C_{\rm RG}^{\xi} \sqrt{T/B} \, e^{B/T}, \qquad (1)$$

where Δ is the lattice constant, $B = \sqrt{3}\,\pi(\pi/4 + \frac{1}{2}) = 6.994$. The prefactor $C_{\rm RG}^{\xi}$ is left undetermined by the RG calculation.

It follows from topological considerations that the order-parameter field of the HAFT allows for excitations of the form of Z_2 vortices.[7,8] A numerical study of the classical HAFT (Ref. 7) has revealed that these vortices become abundant above a threshold temperature $T_{\rm th} \simeq 0.3$ and that they

unbind for $T > T_{\rm th}$, similarly as the Z vortices in the planar XY model above the Kosterlitz-Thouless (KT) transition temperature $T_{\rm KT}$.[9] Further evidence for this similarity between the dissociation mechanism of the Z_2 vortices and that of the Z vortices has been provided by Kawamura and Kikuchi.[10] In recent work,[11] we have studied the influence of the vortices on the partition function of the classical HAFT on the basis of the NLσ model. While a true KT-type phase transition can be ruled out for the HAFT, our results suggest that for $T > T_{\rm th}$ the vortices will affect the properties of the HAFT rather drastically. In particular, the disorder induced by the unbinding of the vortices can be expected to lead to a crossover from the T-dependence Eq. (1) of the correlation length in the low-temperature regime $T < T_{\rm th}$ to a KT-type behavior

$$\xi = \Delta C_{\rm KT}^{\xi} \exp[b/(T - T_{\rm th})^{1/2}] \qquad (2)$$

in the high-temperature regime.

It is the aim of the present paper to supplement our recent analytical study,[11] which was based on a continuum description of the HAFT by a Monte Carlo (MC) simulation of the original lattice model. A similar study has recently been published by Southern and Young.[12] While we closely follow the method of these authors, our conclusions will be quite different from theirs.

In the next section, we first give a brief account of the technique we used. Subsequently we present the results for the correlation length ξ and the antiferromagnetic susceptibility $\chi(\mathbf{Q})$. While these quantities are directly accessible to simulations in the high-temperature regime, where the disordering effect of the vortices limits the range of the correlations, the key quantity to be computed in the low-temperature regime is the spin stiffness.[13,12] Our numerical results for this last quantity will be presented and discussed in Sec. III. Finally, we summarize the evidence for a vortex induced crossover transition in Sec. IV.

II. CORRELATION LENGTH AND ANTIFERROMAGNETIC SUSCEPTIBILITY

The classical Hamiltonian of the triangular Heisenberg antiferromagnet can be defined as

$$H = \sum_{\langle i,j \rangle} \mathbf{S}_i \cdot \mathbf{S}_j. \tag{3}$$

Here, the $\mathbf{S}_i$ are three-dimensional unit vectors and the sum extends over all distinct pairs of nearest neighbor sites of a triangular lattice of L^2 sites. The exchange constant has been set to unity. The classical ground state of the Hamiltonian Eq. (3) is a coplanar arrangement in which the spins on the three sublattices are oriented at $120°$ relative to each other,

$$\mathbf{S}_i = \mathbf{e}_1 \cos(\mathbf{Q}\mathbf{R}_i) + \mathbf{e}_2 \sin(\mathbf{Q}\mathbf{R}_i). \tag{4}$$

Here, $\mathbf{e}_1$, $\mathbf{e}_2$ are a pair of mutually orthogonal unit vectors and $\mathbf{Q}$ can be any one of the six vectors pointing towards the corners of the hexagonal Brillouin zone of the triangular lattice, e.g., $\mathbf{Q} = (2\pi/\Delta)(\frac{2}{3},0)$. The correlation length ξ can be obtained assuming a Ornstein-Zernicke form for the structure factor

$$S(\mathbf{q}) = \frac{1}{L^2} \sum_{i,j} e^{i\mathbf{q}(\mathbf{R}_i - \mathbf{R}_j)} \langle \mathbf{S}_i \cdot \mathbf{S}_j \rangle \tag{5}$$

$$= \frac{S(\mathbf{Q})}{1 + \xi^2 (\mathbf{q} - \mathbf{Q})^2}.$$

$\chi(\mathbf{Q}) = S(\mathbf{Q})/T$ is then the susceptibility of the system at the ordering wave vector. The spin correlations $\langle \mathbf{S}_i \cdot \mathbf{S}_j \rangle$ in Eq. (5) can be determined by MC techniques. We used the local algorithm described by Kawamura and Miyashita.[7] The lattice is divided into independent sublattices. Then, the spins of each of these sublattices are updated sequentially. For a given spin, a new direction is chosen at random and the standard Metropolis rule is used to decide whether the new direction is to be accepted. If it is discarded, a precessional motion through a randomly chosen angle about the direction of the local mean field is performed. We apply this method to systems of linear sizes $L = 12 \times 2^n, n = 0,1, \ldots ,5$. For the smaller systems, $n \leq 3$, we discard the first 2×10^4 sweeps for equilibration and average over the next 2×10^5 sweeps. For $n = 4$, we average over 4×10^5 sweeps after discarding the initial 10^5 sweeps, and for $n = 5$, the average is over 1.8×10^6, and 2×10^5 sweeps are discarded.

A selection of results for the correlation length ξ and for the antiferromagnetic susceptibility $\chi(\mathbf{Q})$ which have been obtained by averaging over 3–5 independent runs of these lengths is tabulated in Table I. As will become apparent shortly, the data shown in this table are crucial in checks of theoretical predictions for the temperature dependence of ξ and $\chi(\mathbf{Q})$. To exhibit possible finite size effects, Table I contains two pairs of data for each temperature which correspond to two different system sizes L, $2L$. In general, ξ and $\chi(\mathbf{Q})$ decrease with T, but increase with the system size L. If, for a given temperature T_0 and a given system size L_0, the data for ξ and $\chi(\mathbf{Q})$ exhibit no size dependence upon doubling the system size, then one can conclude that the system size L_0 suffices to obtain size independent data for all $T > T_0$. Data which are size independent by this criterion are

TABLE I. Correlation length ξ and antiferromagnetic susceptibility $\chi(\mathbf{Q})$ for system sizes $L = 96$, 192, and 384 for various temperatures. The statistical error represents the standard deviation over 3–5 independent runs. The two last columns contain the RG predictions for ξ and $\chi(\mathbf{Q})$. Asterisks indicate agreement of the results for different system sizes, see main text.

T	L		ξ	χ	ξ_{RG}	χ_{RG}
0.300	384		105.0 ± 11.9	5014 ± 543		
0.300	192		83.5 ± 3.5	2800 ± 135	82.8	3609
0.305	384	*	60.7 ± 6.7	2184 ± 273		
0.305	192		63.4 ± 3.8	1899 ± 55	57.0	1796
0.310	192		41.3 ± 1.8	1040 ± 39		
0.310	96		38.2 ± 0.3	748 ± 20	39.7	914
0.315	192		31.7 ± 1.1	594 ± 25		
0.315	96		29.3 ± 0.7	494 ± 11	28.0	476
0.320	192	*	22.7 ± 2.0	349 ± 27		
0.320	96		22.6 ± 1.1	350 ± 13	19.9	253
0.330	192	*	14.3 ± 3.4	169 ± 17		
0.330	96		14.5 ± 1.5	169 ± 9	10.4	76
0.340	192	*	11.8 ± 3.3	103 ± 7		
0.340	96		9.8 ± 1.1	96 ± 5	5.7	25

marked by an asterisk in Table I. Obviously, we cannot exclude that the data for the lowest temperature $T = 0.3$ obtained for the $L = 384$ system are still size dependent. Certainly, however, our data for $T = 0.3$ are lower bounds to the thermodynamic limits of ξ and $\chi(\mathbf{Q})$ at this temperature. To facilitate the comparison of our data with the RG predictions we include in Table I the values for ξ and $\chi(\mathbf{Q})$ which result from fits of the expressions Eq. (1) and Eq. (6), to these data.[12]

In Figs. 1 and 2, we show our complete sets of results for the correlation length and for the antiferromagnetic susceptibility as functions of the temperature. Obviously, for any given system size L, there is an inflection point in the sequences of data for ξ and $\chi(\mathbf{Q})$. This point defines a temperature T_L below which both ξ and $\chi(\mathbf{Q})$ begin to exhibit finite size effects. In fact, as can be seen in Fig. 1, the correlation length increases linearly with the system size for sufficiently low temperatures $T \ll T_L$. Figures 1 and 2 also contain fits of different theoretical predictions to the numerical data. The dashed lines represent fits of the RG result, Eq. (1), to our data for ξ and of the form

$$\chi(\mathbf{Q}) = C_{RG}^{\chi}(T/B)^4 \exp(2B/T), \tag{6}$$

proposed by Southern and Young[12] on the basis of RG calculations, to our data for $\chi(\mathbf{Q})$. In these RG predictions, the constants C_{RG}^{ξ} and C_{RG}^{χ} are the only undetermined parameters. In our fits, we neglect the data points for temperatures $T \leq T_L$ which contain finite size effects. In agreement with Southern and Young[12] we find $C_{RG}^{\xi} \simeq 3 \times 10^{-8}$ and $C_{RG}^{\chi} \simeq 6 \times 10^{-12}$. The solid lines represent fits of the KT forms Eq. (2) and

$$\chi(\mathbf{Q}) = C_{KT}^{\chi} \exp[\tfrac{7}{4} \cdot b/(T - T_{th})^{1/2}] \tag{7}$$

to the data. With the KT form for ξ, Eq. (2), the last expression follows from the general relation $S(\mathbf{Q}) \sim \xi^{2-\eta}$ for the
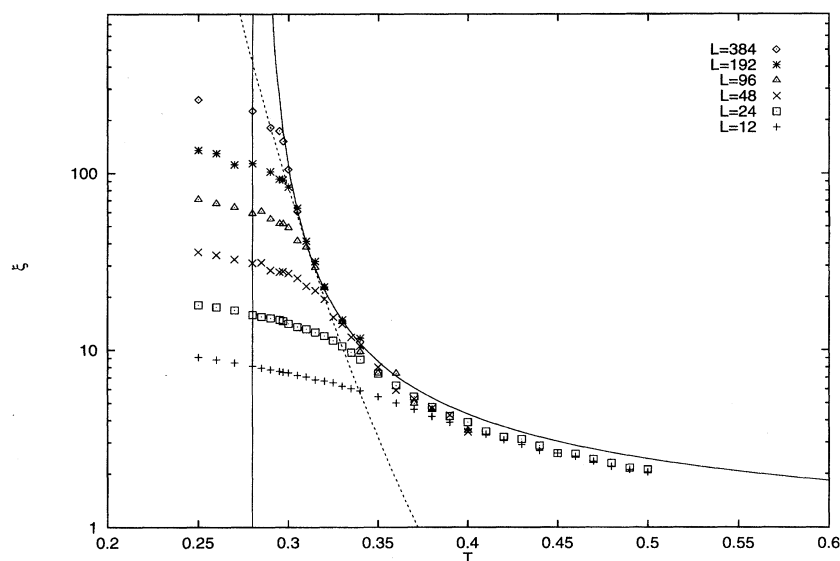
FIG. 1. Correlation length ξ as a function of the temperature T. Solid line: the KT form Eq. (2) with $C_{KT}^{\xi}=0.47$, $b=0.77$, and $T_{th}=0.28$. Dashed line: the RG behavior Eq. (1) with $C_{RG}^{\xi}=3\times10^{-8}$.

structure factor at the ordering wave vector, if η is assumed to take the value $\eta=1/4$ as for a proper KT transition. For the threshold temperature, we use the value $T_{th}=0.28$, which can be inferred from the temperature dependence of the spin stiffness as will be discussed in the next section. This leaves the constant b which is common to expressions (2) and (7) and the constant factors C_{KT}^{ξ} and C_{KT}^{χ} of Eq. (2) and Eq. (7) as fit parameters. As before, we ignore data points for $T \leq T_L$ in our fits. The results are $b=0.77$, $C_{KT}^{\xi}=0.47$, and $C_{KT}^{\chi}=0.40$. Obviously, for temperatures $T \geq 0.3$, the $\exp[b/(T-T_{th})^{1/2}]$ temperature dependence of the KT forms fits the data better than the $\exp(B/T)$ temperature dependence predicted by the RG analysis. In Figs. 3 and 4 we plot ξ and $\chi(\mathbf{Q})$ logarithmically against $(T-T_{th})^{-1/2}$ so that the KT forms, Eq. (2) and Eq. (7) appear as straight lines. These lines are seen to fit the data quite well in the temperature interval $0.30 \leq T \leq 0.34$, whereas the agreement between the

curves representing the RG forms is restricted to a narrow interval around $T \approx 0.31$. In particular, we emphasize that for $T=0.3$, the RG predictions are incompatible with the data points for ξ and $\chi(\mathbf{Q})$ which are listed in Table I with their respective errors. In this context, we recall that if our data for $T=0.3$ do not represent the thermodynamic limits of ξ and $\chi(\mathbf{Q})$, they are certainly lower bounds to these limits. Hence, the discrepancy between the RG predictions and the true values of ξ and $\chi(\mathbf{Q})$ may even be larger than has been inferred here. We note that the fit of the KT form, Eq. (7), to the data for the susceptibility $\chi(\mathbf{Q})$ is better than that of the RG form, Eq. (2), to ξ. This may be attributable to the lower quality of the data for ξ which are obtained indirectly from the Ornstein-Zernicke expression, Eq. (5), in the limit $\xi|\mathbf{Q}-\mathbf{q}| \ll 1$.

In summary, we observe that our results combined with the earlier findings of Kawamura and Miyashita[7] support the
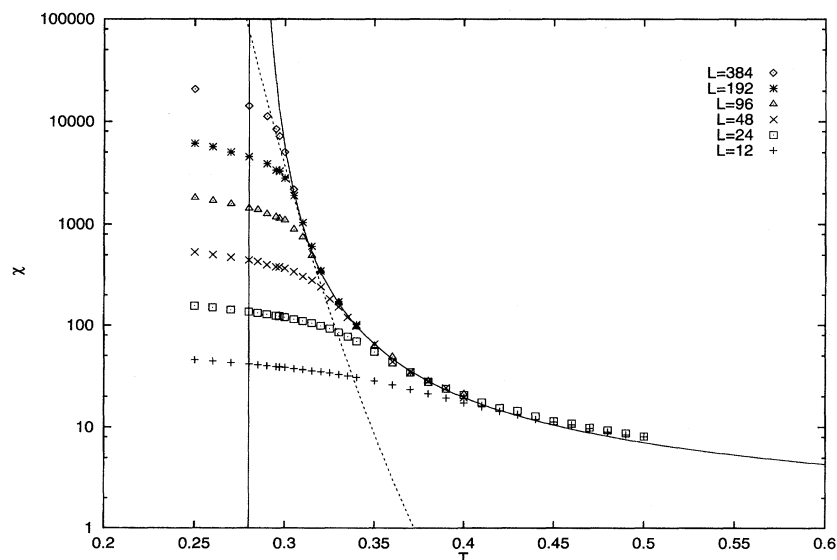

FIG. 2. Antiferromagnetic susceptibility $\chi(\mathbf{Q})$ as a function of the temperature T. Solid line: the KT form Eq. (7) with $C_{KT}^{\chi}=0.40$, $b=0.77$, and $T_{th}=0.28$. Dashed line: the RG behavior Eq. (6) with $C_{RG}^{\chi}=6\times10^{-12}$.
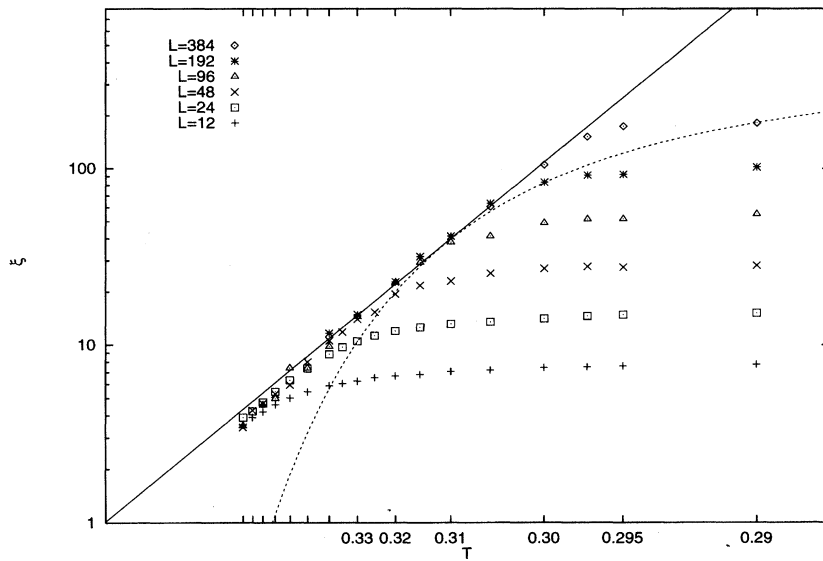
FIG. 3. Correlation length ξ as a function of $(T-T_{\text{th}})^{-1/2}$. The lines are defined as in Fig. 1.

view that in the temperature range $T > T_{\text{th}}$ the spin correlations of the HAFT are decisively influenced by unbound vortices, so that a perturbative treatment of the model is inadequate in this temperature regime. It should be obvious, however, that in the above analysis of our numerical results we have been guided by our previous prediction[11] that, in the case of the HAFT, the vortex unbinding mechnism leads to a KT-type temperature dependence of the correlation length above a crossover temperature T_{th}. While we do not claim to have found compelling evidence for this prediction, we regard our numerical results as strong support for it.

III. SPIN STIFFNESS

To further corroborate the above view and in order to get insight into the low-temperature regime, where the correlation length exceeds the accessible system sizes, we also de-

termined the spin stiffness ρ in our simulations.

The diagonal components ρ_α, $\alpha = 1,2,3$, of the spin stiffness tensor are the second derivatives of the free energy density $f(\theta_\alpha)$ with respect to the twist angles θ_α of the spins around three mutually orthogonal axes e_α,[13,12]

$$\rho_\alpha = -\frac{2}{\sqrt{3}L^2}\left\langle \sum_{\langle i,j \rangle} [\mathbf{S}_i \cdot \mathbf{S}_j - (\mathbf{S}_i \cdot \mathbf{e}_\alpha)(\mathbf{S}_j \cdot \mathbf{e}_\alpha)](\mathbf{u} \cdot \mathbf{e}_{ij})^2 \right\rangle$$

$$-\frac{2}{\sqrt{3}TL^2}\left\langle \left[\sum_{\langle i,j \rangle} \mathbf{S}_i \times \mathbf{S}_j \cdot \mathbf{e}_\alpha(\mathbf{u} \cdot \mathbf{e}_{ij}) \right]^2 \right\rangle . \quad (8)$$

Here, $\mathbf{u}$ is the lattice direction along which the twist is applied and $\mathbf{e}_{ij}$ is the direction of the bond between nearest neighbor lattice sites i and j. The prefactor in Eq. (8) has been chosen such that Eq. (8) is the stiffness per unit area.
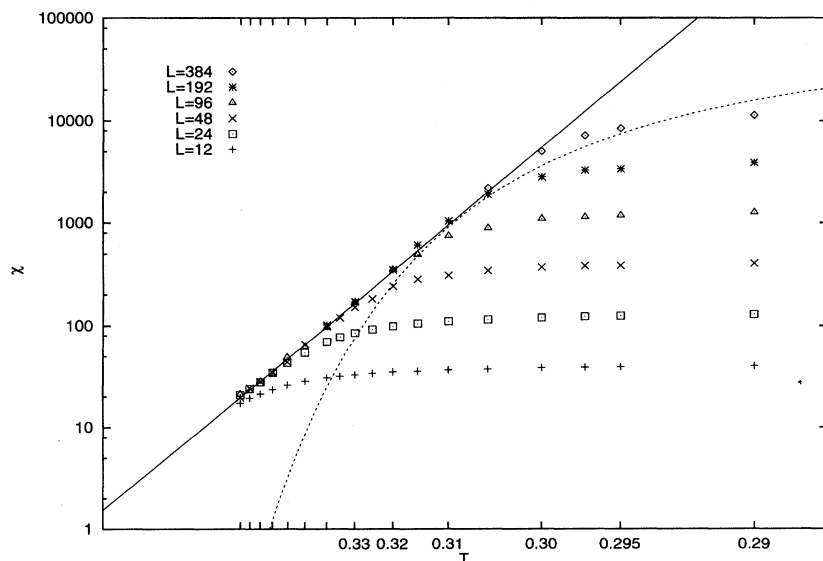

FIG. 4. Antiferromagnetic susceptibility $\chi(\mathbf{Q})$ as a function of $(T-T_{\text{th}})^{-1/2}$. The lines are defined as in Fig. 2.
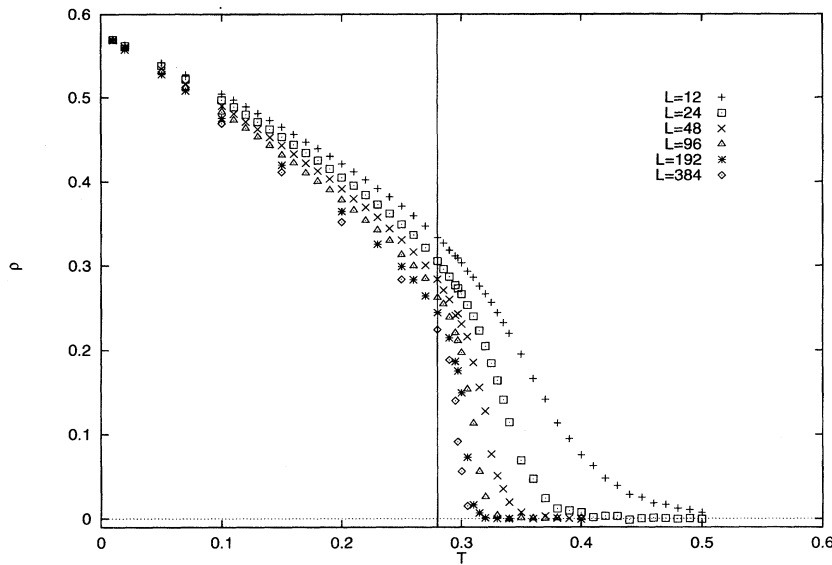
FIG. 5. Spin stiffness ρ as a function of the temperature T.

In the simulation, the thermal averages on the right-hand side of Eq. (8) are replaced by averages over configurations which are generated by a large number of successive MC sweeps. For a finite system, the ordered spin structure will change its orientation in space in the course of the simulation. In a sufficiently large number of sweeps, one will therefore measure the average spin stiffness

$$\rho = \tfrac{1}{3} \sum_{\alpha=1}^{3} \rho_\alpha. \qquad (9)$$

Since there is no long range order in the HAFT for any finite temperature, ρ must vanish for the HAFT in the thermodynamic limit for any finite temperature. However, for finite system sizes L, ρ will be finite for sufficiently low temperatures such that $\xi > L$. According to Eq. (1), this condition should be satisfied for system sizes $L < 10^3$ up to tempera-

tures of the order of unity, unless the constant C_{RG}^{ξ} is exceedingly small as has been suggested by Southern and Young.[12] As we have argued above, the results for ξ in the high-temperature regime, $T > T_{th}$, should not be interpreted as evidence for such a small value of C_{RG}^{ξ}. In fact, a naive integration of the two-loop renormalization-group equations which starts with the microscopic parameters of the HAFT as initial values yields the result Eq. (1) with C_{RG}^{ξ} $= \sqrt{(\pi/4 + 1/2)}e^{-(\pi/4 + 1/2)} = 0.314$.

In our simulations, we determine the three ρ_α separately in each sweep and thus obtain the averages ρ for each sweep. In Fig. 5, we show the average spin stiffness as a function of the temperature for system sizes $L = 12,24,\ldots,384$. The steep drop in ρ which occurs as T increases beyond $T_{th} \simeq 0.28$ is consistent with the rapid decrease of ξ in the same temperature regime in which the vortices become
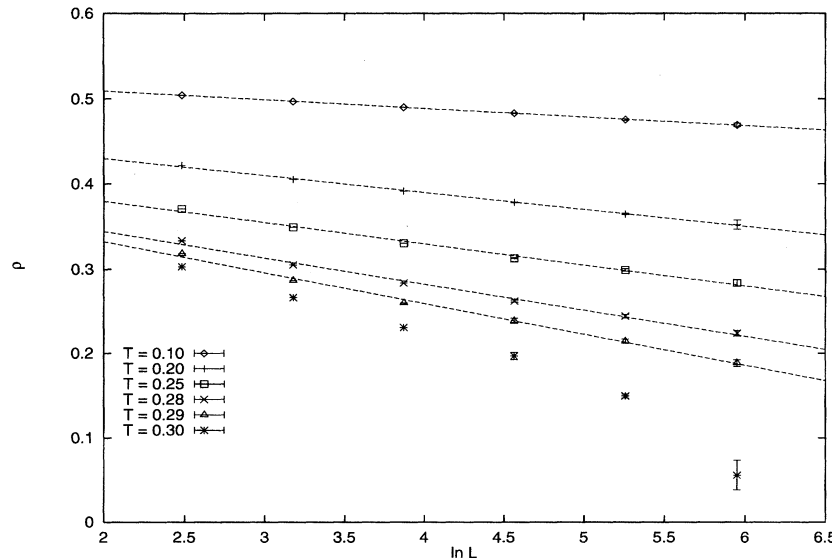

FIG. 6. Spin stiffness ρ as a function of the system size L. The straight lines are mean squares fits, their slopes are tabulated in Table II.
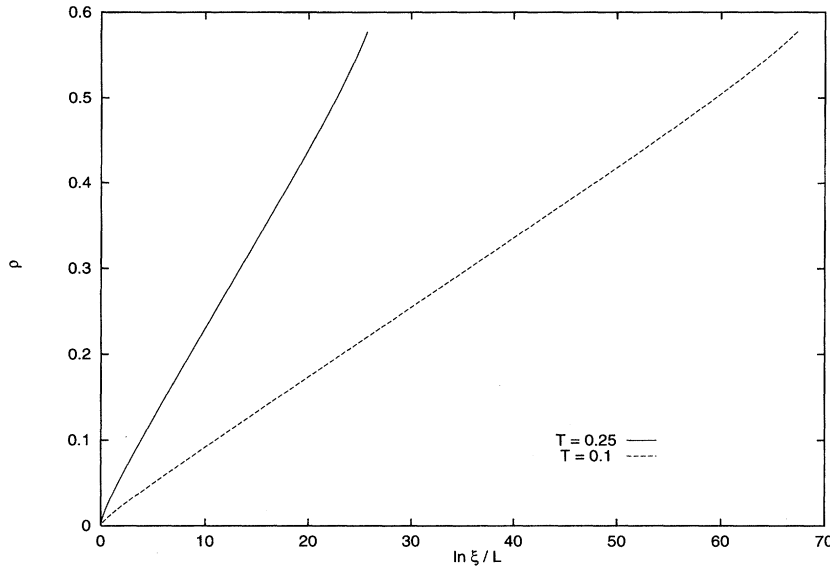
FIG. 7. Spin stiffness ρ as a function of $\ln(\xi/L)$ as obtained from the two-loop RG equations. The curves correspond to $T=0.1$ and 0.25, respectively.

unbound.[7] In contrast to the spin stiffness of the planar XY model, ρ does not saturate in the low-temperature regime $T<T_{th}$ with increasing system size L but decreases with increasing L. This behavior is to be expected, since in contrast with the correlation length of the XY model, the correlation length of the HAFT remains finite for low temperatures, where the vortices are bound in pairs. As $T\rightarrow 0$, our data for ρ approach the correct limiting value $1/\sqrt{3}$.

In Fig. 6, we display ρ for various temperatures and system sizes. The data are averages over 3–5 independent runs of lengths comparable to those which we have described above, error bars indicate the standard deviation.

In the low-temperature regime, the thermodynamics of the classical HAFT should be captured by the appropriate NLσ model.[14,3,4] On the basis of a renormalization-group treatment of this model, Azaria et al.[15] have made detailed predictions for the dependence of the spin stiffness on the linear system size L and the correlation length ξ. In their MC study of the classical HAFT, Southern and Young[12] found excellent agreement with the predicted L dependence of the spin stiffness tensor at the temperature $T=0.2$.

In order to be able to compare our numerical results with the predictions of the RG analysis of the NLσ model, we integrated the two-loop RG equations of Azaria et al.[15] starting from the initial conditions $\rho(L=\Delta)=1/\sqrt{3}$ and $\rho_3(L=\Delta)/\rho_1(L=\Delta)=2$. Here, ρ_1 and ρ_3 are the two main components of the spin stiffness tensor with respect to the reference frame of the local order parameter.[12] By the above initial conditions we identify ρ_1 and ρ_3 with their microscopic values on the scale of the lattice constant Δ. We find that in the temperature regime under consideration, $T\leqslant 0.3$, the average stiffness ρ varies linearly with $\ln L$ to a very good approximation on the scale $12\leqslant L\leqslant 384$ covered by our simulations, see Fig. 7 below. From the RG equations, one can also infer that the slope $\rho'(L)=-d\rho(L)/d\ln L$ decreases from $\rho'=T/(3\pi)$ to $\rho'=T/(4\pi)$, when L increases from a value of the order of the lattice constant, $L\sim\Delta$, to a value of the order of the correlation length, $L\sim\xi$. In Fig. 6, the straight lines are least squares fits to the data. The slopes of

these lines, normalized to the maximal theoretical slope $\rho'=T/(3\pi)$, are tabulated in Table II. For $T\leqslant 0.25$, the slopes are seen to be rather close to their maximal value which obtains, when L is of the order of the lattice constant. This is not unexpected since according to the RG calculations, the correlation length is many orders of magnitude larger than our maximal system size $L=384$ for these temperatures. The larger values of ρ' which we find for $T\geqslant 0.28$ are incompatible with the RG theory. Hence we conclude that for $T\geqslant 0.28$ unbound vortices, not being taken into account by the RG analysis, begin to limit the range of the spin correlations in the HAFT.

If one defines the correlation length ξ through the matching condition $\rho(L=\xi)=0$, then the result of the integration of the two-loop RG equations can be cast into the following form:

$$\rho=f(T,L)\ln(\xi/L). \tag{10}$$

This is shown for two different temperatures in the two graphs in Fig. 7. Obviously, the function $f(T,L)$ depends weakly on L. The relation Eq. (10) makes it possible to obtain the correlation length from the Monte Carlo simulation, even in the low-temperature regime where ξ is much larger than the system size L. Inserting our MC data for ρ into Eq. (10) and solving for ξ, we obtain the data points shown in Fig. 8 for $T\leqslant 0.28$. This figure also includes the data for $T\geqslant 0.28$ which have already been shown in Fig. 1. The dashed and solid lines in Fig. 8 represent fits of the RG and KT forms, Eqs. (1) and (2), to the MC data for $T\leqslant 0.28$ and $T\geqslant 0.28$, respectively.

TABLE II. Slopes of the fits in Fig. 7 normalized to the maximum slope $T/(3\pi)$.

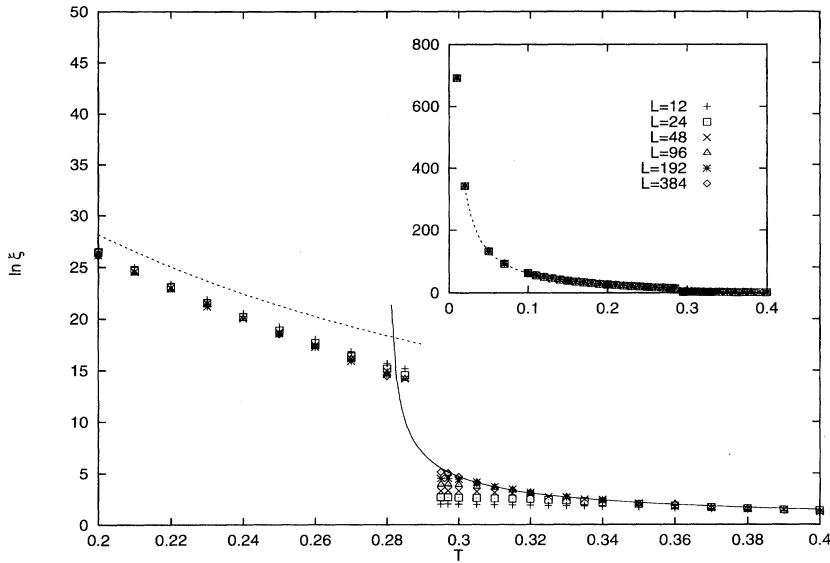| T	0.10	0.20	0.25	0.28	0.29	0.30
ρ'/ρ'_{max}	0.962	0.937	0.939	1.045	1.191	2.098

FIG. 8. Correlation length as a function of the temperature. Dashed lines: fit of the RG result to the low-temperature data. Solid line: fit of the KT form to the high-temperature data. The inset shows the data on a larger temperature scale.

IV. SUMMARY

We have shown that the MC simulation of the HAFT yields compelling evidence for the influence of vortices on the spin correlations and hence on the thermodynamics of this model. In agreement with earlier findings by Kawamura and Miyashita[7] we find that the disordering effect of the vortices sets in rather abruptly at a temperature $T_{th} \simeq 0.28$. Up to this temperature, our data for the spin stiffness ρ and the ensuing temperature dependence of the correlation length ξ are consistent with the predictions of the RG analysis of the HAFT which ignores the existence of topological defects such as vortices. For $T > T_{th}$, however, the simulation yields temperature dependences of the correlation length ξ and the antiferromagnetic susceptibility $\chi(\mathbf{Q})$ which are incompatible with the RG predictions. Instead, in this temperature regime, the temperature dependences of ξ and $\chi(\mathbf{Q})$ which follow from the KT picture of unbinding vortex pairs provide satisfactory fits of the data. A rapid increase of the density of unbound vortices for $T > 0.3$ had already been found by Kawamura and Miyashita in their simulation of the HAFT.[7] It had not been clear, however, whether this phenomenon would lead to the same temperature dependences of the correlations of the HAFT as had been predicted for the planar XY model by Kosterlitz and Thouless.[9] In our recent analytical study,[11] we were led to the conclusion that this should indeed be the case. The present numerical study fully supports this conclusion. As we have discussed in Ref. 11, the crossover transition from the RG-type behavior to the KT type behavior of the correlations of the HAFT cannot imply a phase transition in the proper sense, because the correlation length is finite both below and above the transition temperature T_{th}. The results shown in Fig. 8 indicate, however, that the transition happens in a very narrow interval around T_{th}. Therefore we consider it possible that the derivative of the correlation length with respect to the temperature develops a discontinuity at T_{th} in the thermodynamic limit.

ACKNOWLEDGMENT

[1] H. Kadowaki, H. Kikuchi, and Y. Ajiro, J. Phys. C 2, 4485 (1990); K. Takeda, K. Miyake, K. Takeda, and H. Hirakawa, J. Phys. Soc. Jpn. 61, 2156 (1992); N. Kojima et al., J. Phys. Soc. Jpn. 62, 4137 (1993).

[2] P. Azaria, B. Delamotte, and T. Jolicoeur, Phys. Rev. Lett. 64, 3175 (1990).

[3] P. Azaria, B. Delamotte, and D. Mouhanna, Phys. Rev. Lett. 68, 1762 (1992).

[4] W. Apel, M. Wintel, and H. U. Everts, Z. Phys. B 86, 139 (1992).

[5] P. Leung and K. Runge, Phys. Rev. B 47, 5861 (1993).

[6] B. Bernu, C. Lhuillier, and L. Pierre, Phys. Rev. Lett. 69, 2590 (1992); R. Deutscher and H. U. Everts, Z. Phys. B 93, 77 (1993); B. Bernu, P. Lecheminant, C. Lhuillier, and L. Pierre, Phys. Rev. B 50, 10 048 (1994).

[7] H. Kawamura and S. Miyashita, J. Phys. Soc. Jpn. 53, 4138 (1984).

[8] N. Mermin, Rev. Mod. Phys. 51, 591 (1979).

[9] J. M. Kosterlitz and D. J. Thouless, J. Phys. C 6, 1181 (1973).

[10] H. Kawamura and M. Kikuchi, Phys. Rev. B 47, 1134 (1993).

[11] M. Wintel, H. U. Everts, and W. Apel, Europhys. Lett. 25, 711 (1994).

[12] B. W. Southern and A. Young, Phys. Rev. B 48, 13 170 (1993).

[13] M. Caffarel, P. Azaria, B. Delamotte, and D. Mouhanna, Europhys. Lett. 26, 493 (1994).

[14] T. Dombre and N. Read, Phys. Rev. B 39, 6797 (1989).

[15] P. Azaria, B. Delamotte, T. Jolicoeur, and D. Mouhanna, Phys. Rev. B 45, 12 612 (1992).